Emergence of diverse lanthanum fluorides under high pressure: From insulators to half-metals and superconductors

Ziji Shao,[1] Changqiu Yu,[1] Menghao Jin,[1] Jiahong Wen,[1] Haodong Fan,[1] Bo Liu,[2,*] and Tiejun Zhou[1,2,†]

[1]*Center for Integrated Spintronic Devices, Hangzhou Dianzi University, Hangzhou 310018, China*

[2]*Key Laboratory of Spintronics Materials, Devices and Systems of Zhejiang Province, Zhejiang 311305, China*

(Received 14 June 2023; accepted 26 July 2023; published 9 August 2023)

We present a comprehensive first-principles investigation of the La-F system in rare-earth fluorides under pressures ranging from 50 to 300 GPa. Our study reveals the existence of novel F-rich phases LaF_5 and LaF_6 with F-43m and $R3$ symmetry, respectively, in addition to the known insulating LaF_3. LaF_5, a binary derivative of half-Heusler alloys, exhibits half-metallic ferromagnetism between 14 and 100 GPa, with large band gaps of 5.7–6.9 eV of the spin-up channel and high Curie temperatures of 673–505 K. Electronic analysis attributes the ferromagnetic and half-metallic properties to F atoms in tetrahedral motifs. Furthermore, we predict that trigonal LaF_6, characterized by layered stacking structures, exhibits superconductivity with a critical temperature (T_c) of 5 K at 50 GPa. Our findings provide valuable insights into the high-pressure behavior of rare-earth fluorides and their potential applications in advanced materials and devices.

DOI: 10.1103/PhysRevB.108.064411

I. INTRODUCTION

The behaviors of fluorides under high pressures have garnered significant interest in exploring unconventional chemical regimes and uncovering remarkable physical properties. Because of the highest electronegativity in the periodic table of elements, fluorine can oxidize other elements in compounds [1]. Under high pressure, fluorine retains its strong oxidability [2]. Combined with the modification of the orbital energy level induced by pressure [3], fluorine enables the creation of atypical hypervalent states of fluoridized elements breaking the chemical limits at ambient pressure [4–6]. A diversity of F-rich compounds with unusual oxidation states have been found under high pressure. For instance, the +8 hyperoxidation state realized in IF_8, OsF_8, and IrF_8 [5,7,8], +6 states in AuF_6 and RaF_6 [4,9], +5 states in CsF_5 and BaF_5 [10,11], +4 states in HgF_4 [6], and so on.

Rare-earth (RE) fluorides (REF_n) have shown great application value in the area of optical devices [12–14], telecommunication [15], solar cells [16], and biomedical fields [17,18]. Under ambient conditions, REF_n has two typical structures [19,20]. For REs with large ionic radii like LaF_3-NdF_3, the stable crystal structure is described as trigonal P-3c1 phase, namely tysonite form [21,22], while for REs with smaller ionic radii like SmF_3-LuF_3 and YF_3, phase facilitates the β-YF_3 phase with $Pmmn$ symmetry [23]. Experimental and theoretical works have been conducted and found that LaF_3 experiences a phase transition from tysonite to orthorhombic phase with $Pmmn$ symmetry at around 20 GPa and then to a different orthorhombic phase with space group $Cmcm$ above 150 GPa [24–29]. For the REF_n with β-YF_3 phase at ambient condition, a phase transformation from β-YF_3 to hexagonal phase (LaF_3 type) is found in EuF_3, ErF_3, GdF_3, TbF_3, YbF_3, and LuF_3 [30]. To date, the high-pressure studies on REF_n are limited to trifluorides; the phase diagrams of REF_n under pressure are yet to be constructed and need further investigation.

Herein, we choose the La-F system as the testing target and extensively explore the phase diagram of La-F systems with various LaF_n ($n = 1-7$) compositions from 50 to 300 GPa via the evolutionary structure search algorithm. The $Pnnm$ to $Cmcm$ phase transition of LaF_3 is successfully reproduced [24,28] at 141 GPa, which indicates the reliability of our calculations. In addition, hitherto unknown fluorine-rich compounds F-43m-LaF_5 and $R3$-LaF_6 are stabilized above 120 and 50 GPa, respectively. The predicted LaF_5 can be regarded as a binary derivative of the half-Heusler-type structure. From 14 to 100 GPa, LaF_5 has half-metallic ferromagnetism with a large spin-up channel band gap 5.7−6.9 eV and high Curie temperature of 673–505 K. $R3$-LaF_6 comprising the alternating pure F and La-F layers is found to be superconductive with T_c about 4.1−5.0 K at 50 GPa. The diversity of lanthanide fluorides in chemical stoichiometries, crystal structures, and physical properties indicates that REF_n has potential value for exploring novel functional materials under pressure.

II. CALCULATION METHODS

An extensive search for stable LaF_n ($n = 1-7$) compounds was performed within 2−4 formula units between 50 and 300 GPa by the evolutionary algorithm implemented in the USPEX package [31,32]. Sixty structures were created using a random symmetric generator in the first generation; all subsequent generations contained 30 structures and were produced using variation operators (see details in the Supplemental Material [33]). The formation enthalpy of

*Corresponding author: liubo@spinlab.cn

†Corresponding author: tjzhou@hdu.edu.cn

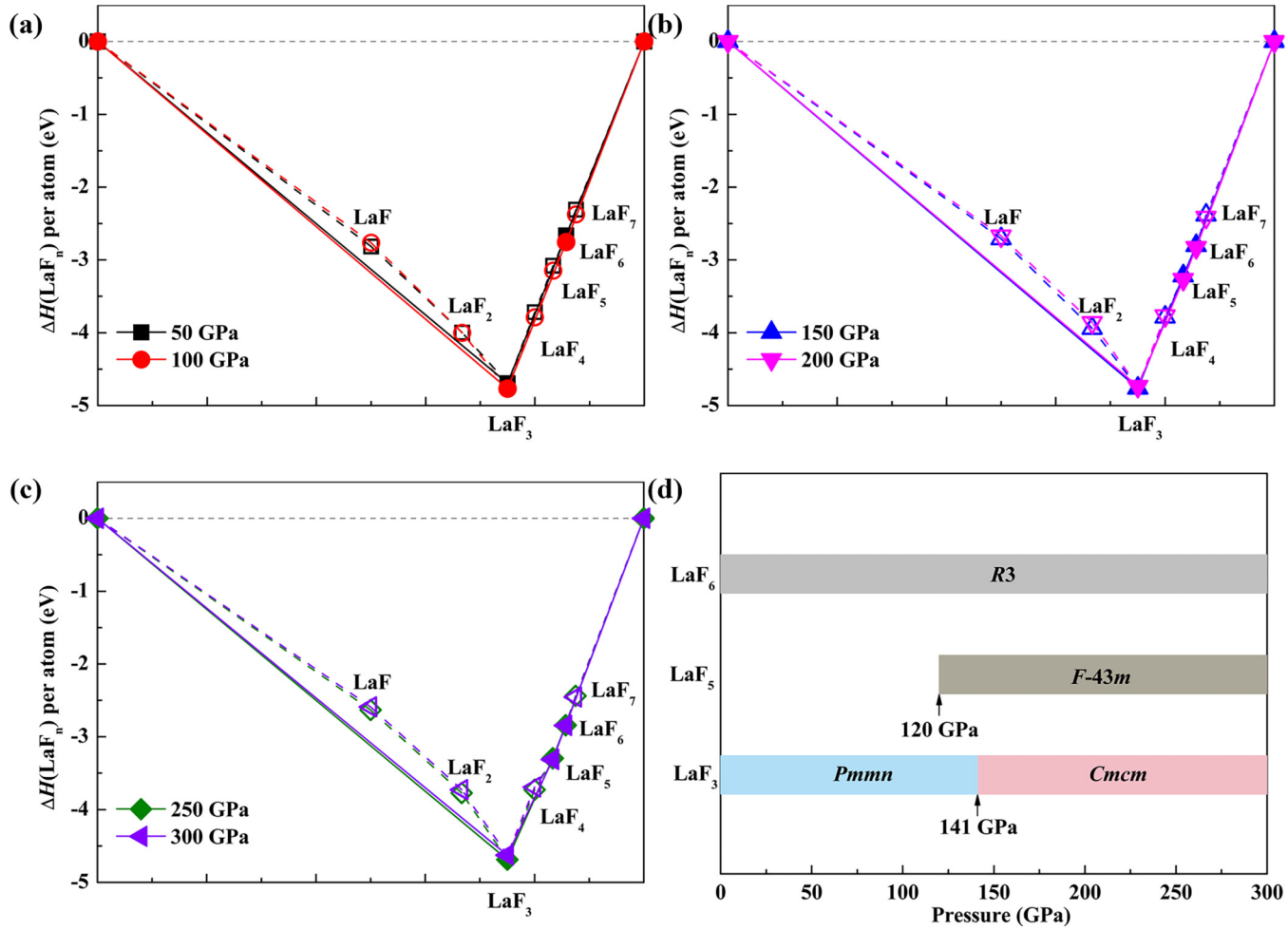

FIG. 1. (a) The enthalpies of formation per atom of LaF_n ($n = 1-7$) with respect to La and F_2 at 50, 100, 150, 200, 250, and 300 GPa. (b) The phase transition series of stable compounds LaF_3, LaF_5, and LaF_6.

LaF_n ($n = 1-7$) $\Delta H(LaF_n)$ per atom with respect to elemental lanthanum and fluorine were calculated according to the following equation: $\Delta H(LaF_n) = E(LaF_n) - E(La) - nE(F)/n + 1$. The Fm-3m-La [34], $I4/mmm$-La [35], and $Cmca$-F_2 [36] structures were adopted as reference structures in their corresponding stable pressure ranges. All the structure relaxations, total energy calculations, electronic properties, and magnetism were conducted in the framework of the density functional theory (DFT) within the Perdew-Burke-Ernzerhof (PBE) exchange-correlation functional [37] as implemented in the VASP package [38]. Ion-electron interactions were described by the projector-augmented wave (PAW) approach [39] with $2s2p$ and $6s5p5d4f$ treated as valence electrons for F and La elements, respectively. The Monkhorst-Pack k mesh with resolution $2\pi \times 0.03$ Å^{-1} was used for calculating enthalpies and elastic constants, and $2\pi \times 0.025$ Å^{-1} for the electronic and magnetic analysis. Based on the DFT calculation by VASP, subsequent calculations were carried out: (i) phonon calculations were conducted by the finite displacement method implemented in the PHONOPY program [40], the $2 \times 2 \times 2$ supercell and the Monkhorst-Pack k mesh with resolution $2\pi \times 0.08$ Å^{-1} were adopted for all the stable structures; (ii) elastic constants were calculated through the strain-stress method [41]; (iii) chemical bonding and charge transfer descriptions were performed with the crystal orbital Hamilton populations (COHP) method as implemented in the LOBSTER package [42] and Bader's quantum theory of atoms in molecules analysis [43], respectively. To investigate the superconductive properties, electron-phonon coupling (EPC) interactions were conducted by density functional perturbation theory (DFPT) as implemented in the Quantum ESPRESSO package [44]. Ultrasoft pseudopotentials for F and La were utilized with a kinetic energy cutoff of 60 Ry. The k- and q-point meshes were $18 \times 18 \times 18$ and $3 \times 3 \times 3$ for $R3$-LaF_6 at 50 GPa. The superconductive transition temperatures T_c were estimated through the Allen-Dynes-modified McMillan equation [45]:

$$T_c = \frac{\omega_{\log}}{1.2} \exp\left[-\frac{1.04(1+\lambda)}{\lambda - \mu^*(1+0.62\lambda)}\right], \quad (1)$$

where the μ^* is the effective Coulomb repulsion, which is usually taken as 0.1–0.13, the EPC parameter λ and the logarithmic average frequency $\omega_{\log}$ are respectively calculated as follows:

$$\lambda = 2\int_0^\infty \frac{\alpha^2 F(\omega)}{\omega} d\omega \quad (2)$$

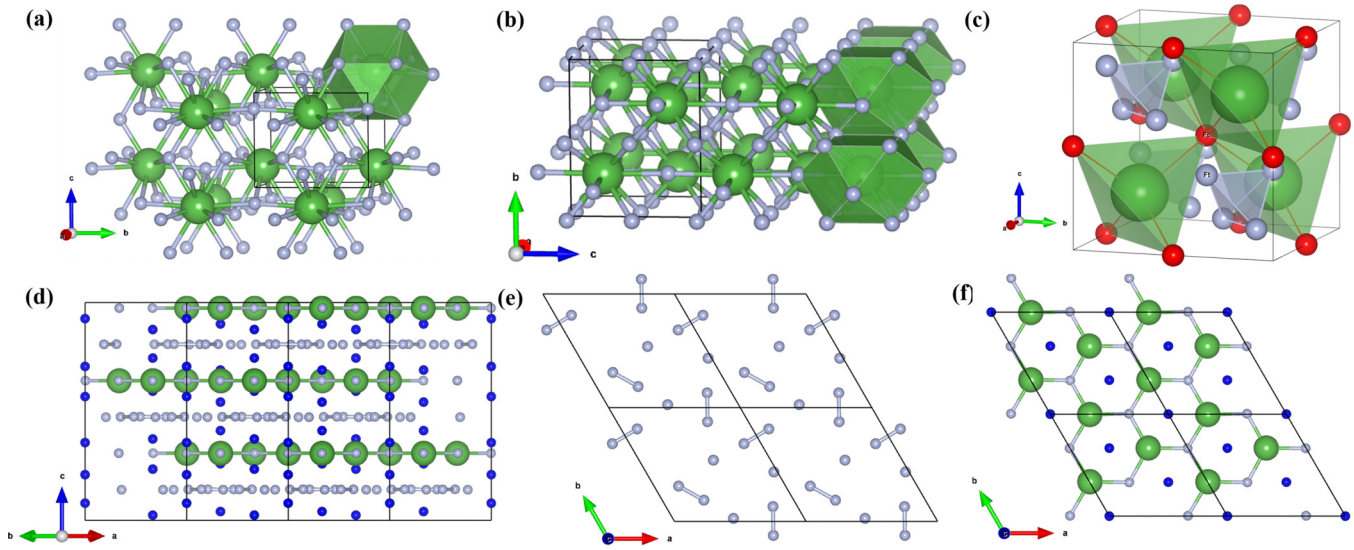

FIG. 2. The crystal structures of (a) *Pmmn*-LaF_3, (b) *Cmcm*-LaF_3. Lanthanum atoms are colored green; fluorine atoms are grey. (c) *F*-43*m*-LaF_5, F_c, and F_t atoms are presented as red and grey small balls, respectively. The (d) side view and (e) top view of the pure F layers, and (f) top view of the La-F layers of *R*3-LaF_6. The fluorine atoms located above and below the flat La-F layers with small shifts are displayed as blue small balls.

and

$$\omega_{\log} = \frac{2}{\lambda}\int_0^{\infty} \frac{\alpha^2 F(\omega)\ln(\omega)}{\omega} d\omega. \tag{3}$$

The contribution of the spin-orbit coupling (SOC) was calculated (see Fig. S1 of the Supplemental Material [33]), and the result shows that the SOC has less influence on the calculations [33]. The equation of states of LaF_3 are calculated using VASP and Quantum ESPRESSO package from 25 to 300 GPa (Fig. S2 [33]); the almost identical results of the two codes indicate the consistency of our calculation [33].

III. RESULTS AND DISCUSSION

A. Stabilities and structures

The thermodynamic stabilities of LaF_n compounds are determined through a convex hull which is built by the calculated formation enthalpies of LaF_n [Fig. 1(a)]. The stoichiometries on the solid line are thermodynamically stable. LaF_3 with traditional stoichiometry maintains the most stable composition in the whole pressure range. In addition, the unexpected compounds with higher fluorine contents LaF_5 and LaF_6 emerge on the convex hull in the pressure ranges 50−300 and 150−300 GPa, respectively. The pressure dependence of enthalpies for structures that are found in our work as well as the selected structures from previous studies are also calculated (Fig. S3 [33]) to ensure the energetic stabilities of our predicted compounds. Further information on the stabilities and phase transitions under pressure is depicted by the composition-pressure phase diagram [Fig. 1(b)]. In agreement with the recent experimental and theoretical works [24,28], LaF_3 is stabilized as the *Pmmn* phase at 50 GPa and transforms to the *Cmcm* phase at 141 GPa. For *Pmmn*-LaF_3 and *Cmcm*-LaF_3, La atoms form the orthorhombic frameworks with F atoms spreading around [Figs. 2(a) and 2(b)]. As pressure increases, the coordination number of La increases from 12 to 13 during the *Pmmn* to *Cmcm* phase transition. LaF_5 can be synthesized above 120 GPa with the space group of *F*-43*m* symmetry [Fig. 2(c)]. The F atoms in *F*-43*m*-LaF_5 are categorized into F_c (small red balls) and F_t (small grey balls). F_c arranges into the cubic close-packaged structures with four La occupying their tetrahedral voids. F_c and La atoms form the typical zinc-blende structure. The other tetrahedral voids are filled by tetrahedrons consisting of four F_t atoms (connected by a solid grey line). If we regard every F_t tetrahedron as a pseudoatom $(F_t)_4$, the discovered LaF_5 can be considered as a binary half-Heusler alloy $La(F_t)_4F_c$. The well-known half-Heusler alloys are conventionally denoted as *XYZ* ternary compounds with C_{1b} crystal structure; *X* and *Y* are always transition metals or alkali metals and *Z* is *sp* block elements [46]. In $La(F_t)_4F_c$, La, $(F_t)_4$, and F_c locate at 4*d* (3/4, 3/4, 3/4), 4*b* (1/4, 1/4, 1/4), and 4*a* (0, 0, 0), respectively. For *Pmmn*-LaF_3, *Cmcm*-LaF_3, and *F*-43*m*-LaF_5, the calculated pseudovalence electron localization functions (ELFs) (Fig. S4) show few electron accumulations between F and F atoms or F and La atoms, which indicates that the interactions between F-F and F-La are mainly ionic [33]. LaF_6 has a thermodynamic stable structure in the form of *R*3 in the whole pressure range of interest. The LaF_6 is formed by the stacking of two kinds of layers [Fig. 2(d)]. One is the pure F layer consisting of a mixture of F atoms and F_2 units [Fig. 2(e)]. The 2D pseudovalence ELF (Fig. S4) illustrates the electronic accumulation between F atoms, which indicates the existence of covalent interaction between F-F bonds in F_2 units [33]. The F-F distances in F_2 units are 1.549 Å at 50 GPa and slightly reduced to 1.520 Å at 300 GPa, which is comparable to the bond length (1.43 Å) of the gas F_2 molecular. The topology of the pure F structural motifs is similar to the F_2 planes in the predicted *P*6/*mcc* structure stable between 2.75 and 4 TPa [47]. The other consists of the honeycomb layer connected by La and F atoms in an ionic manner. Above and below the La-F layer, there are F atomic layers with small shifts in atomic

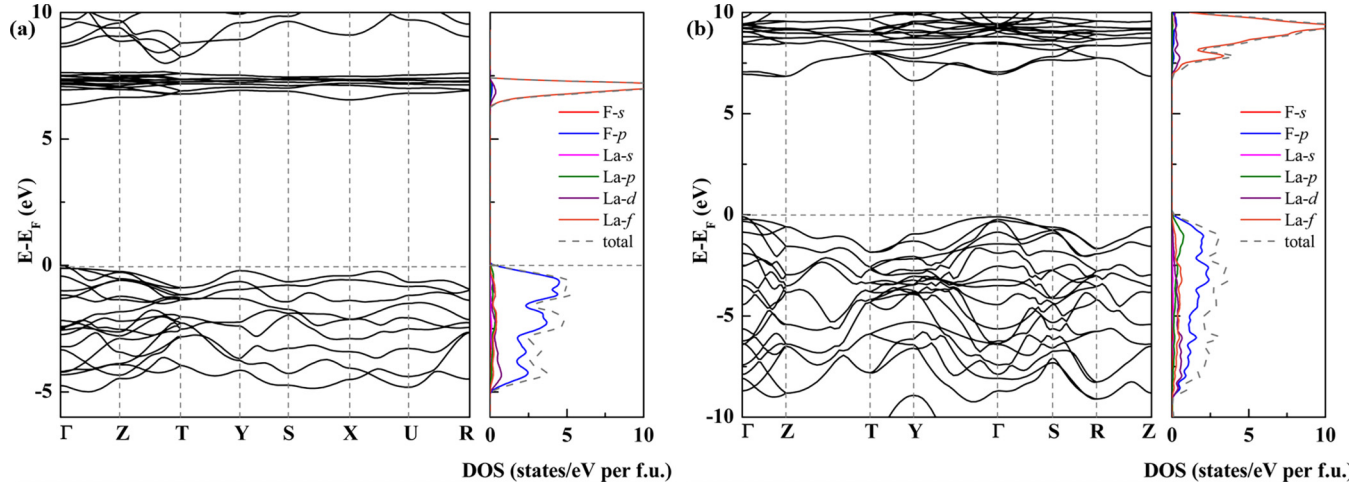

FIG. 3. Electron band structures, the total electron density of states (DOS), and partial electron density of states (PDOS) of (a) *Pmmn*-LaF_3 at 50 GPa and (b) *Cmcm*-LaF_3 at 300 GPa, respectively.

position along the **a** + **b** direction [blue balls in Figs. 2(d) and 2(f)]. The elastic constants and phonon band structures are also calculated (Table SI and Fig. S5 [33]). All the predicted structures are mechanically and dynamically stable in their stable pressure region since the Born stability criteria [48] are met and no imaginary frequency appears in the whole first Brillouin zone. The detailed structural information on the stable structures is provided in Table SII [33]. Since the atypical F-rich stoichiometries are found in LaF_n, the oxidation states of La atoms are also investigated (Fig. S6 [33]). However, according to the analysis of electronic properties, the outmost inner shell $5p$ electrons failed to participate in the bonding interactions and electron transfer, which indicates that the La atoms in LaF_5 and LaF_6 are not hyperoxidized by F atoms under high pressure.

B. Electronic structures and magnetism

The *Pmmn*-LaF_3 are insulators with a direct band gap at the Γ point [Fig. 3(a)]. The band gap is 6.36 eV at 50 GPa. The high-pressure phase *Cmcm*-LaF_3 changed to an indirect band-gap insulator with a band gap of about 6.72 eV at 300 GPa [Fig. 3(b)]. The Bader charge analysis shows that every La atom will donate $3e^-$ to F atoms. According to the partial density of states (PDOS) of *Pmmn*-LaF_3 and *Cmcm*-LaF_3, the highest occupied states are $2p$ orbitals of F and the lowest unoccupied states are $4f$ orbitals of La; the $5d$ and $6s$ electron states of La are rather small under the Fermi level. The results indicate that the valence electrons $5p^16s^2$ of La transform to $2p$ of F. The La^{3+} and F^- ions with fulfilled $4f^{10}$ and $2p^8$ electronic configurations will form the closed-shell structures and reduce the metallic characteristic. The integral COHP (ICOHP) of La-F is about −1.44 to −2.13 and −1.41 to −3.11 eV per pair in *Pmmn*-LaF_3 and *Cmcm*-LaF_3 at 50 and 300 GPa, respectively, while the ICOHP values of F-F bonds are lower than −0.02 eV per pair. Therefore, *Pmmn*-LaF_3 and *Cmcm*-LaF_3 are mainly stabilized through the electron transformation from La to F.

LaF_5 is revealed to be ferromagnetic. The electronic structures at 150 GPa display the F-dominated spin splitting at the Fermi level [Figs. 4(a) and 4(b)], which implies that the magnetism is induced by the partial occupation of the $2p$ states of F atoms. The spin density [inset of Fig. 4(a)] shows that the unpaired electrons accumulate around F_t atoms while F_c is almost nonmagnetic. Bader charges analysis at 150 GPa shows that La loses about $2.20e^-$. The F_c atom gains $0.69e^-$. The almost fulfilled $2p$ orbitals make F_c nonmagnetic. The pseudoatom $(F_t)_4$ gains $1.51e^-$ in total, and every F_t gains almost the same $0.38e^-$. The partial occupation of $2p$ orbitals of F_t induces magnetism. As shown in the spin-restricted COHP of F_t-F_t bonds [Fig. 4(c)], the Fermi level reaches a strong F_t-F_t antibonding region implying the electronic instability of the system. The spin-unrestricted COHP [Fig. 4(d)] shows that spontaneous magnetization makes the spin-up and spin-down electrons inequivalent, reduces the electronic symmetry, annihilates the antibonding states, and then decreases the overall energy [49].

C. Half-metallic ferromagnetism

Most half-metallic ferromagnetism is widely found in Heusler alloys, chalcogenides, and perovskite magnetites [50]. Therefore, the dynamic stability and band structure of LaF_5 under a low-pressure range is also investigated. Phonon band structures imply LaF_5 can be decompressed to 14 GPa (Fig. S7 [33]). When pressure is lower than 100 GPa, ferromagnetic LaF_5 becomes half-metallic with the spin-down channel behaving as a metal while the spin-up band structure possesses a gap [51] (Fig. 5). Theoretically, the DOS at the Fermi level has 100% spin polarization, which has potential applications in spintronic devices such as magnetic tunnel junctions [52,53] and high-efficiency magnetic sensors [54]. The PDOS (Fig. 6) and integral PDOS (IPDOS) for the $2p$ orbitals of $(F_t)_4$ before and after combination with La and F_c indicate that the half-metallic ferromagnetism mainly comes from the $(F_t)_4$ units. The pure $(F_t)_4$ framework without interaction with La and F_c is found to be half-metallic with magnetic momentum of about $4\mu_B$ provided by the unequal occupation of the spin-up and spin-down $2p$ states. The IPDOS of every F_t $2p$ state is about $3e^-$ for the spin-up channel,

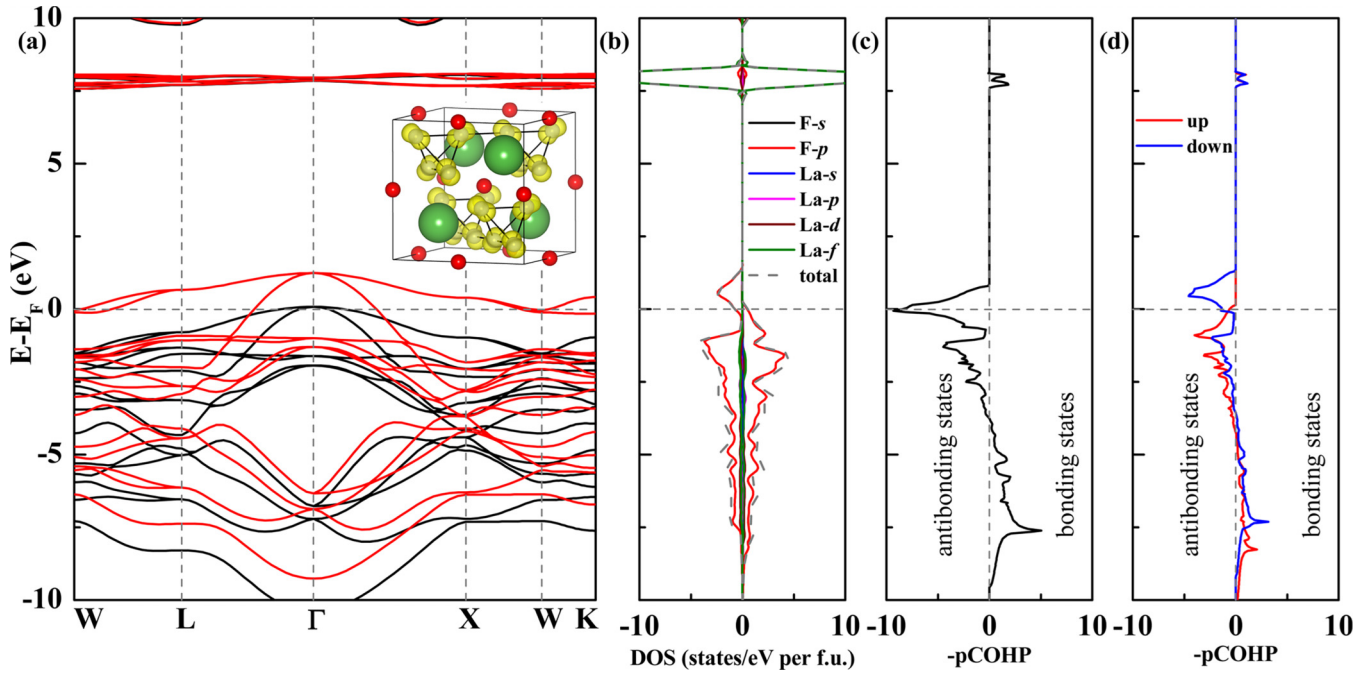

FIG. 4. (a) Electron band structure with spin polarization (spin-up channel and spin-down channel are shown as black and red solid lines), the inset is the 3D spin density. (b) Total and partial electron density of states (DOS and PDOS) with spin polarization, COHP of between F_t atoms (c) without and (d) with spin polarization of F-43m-LaF_5 at 150 GPa.

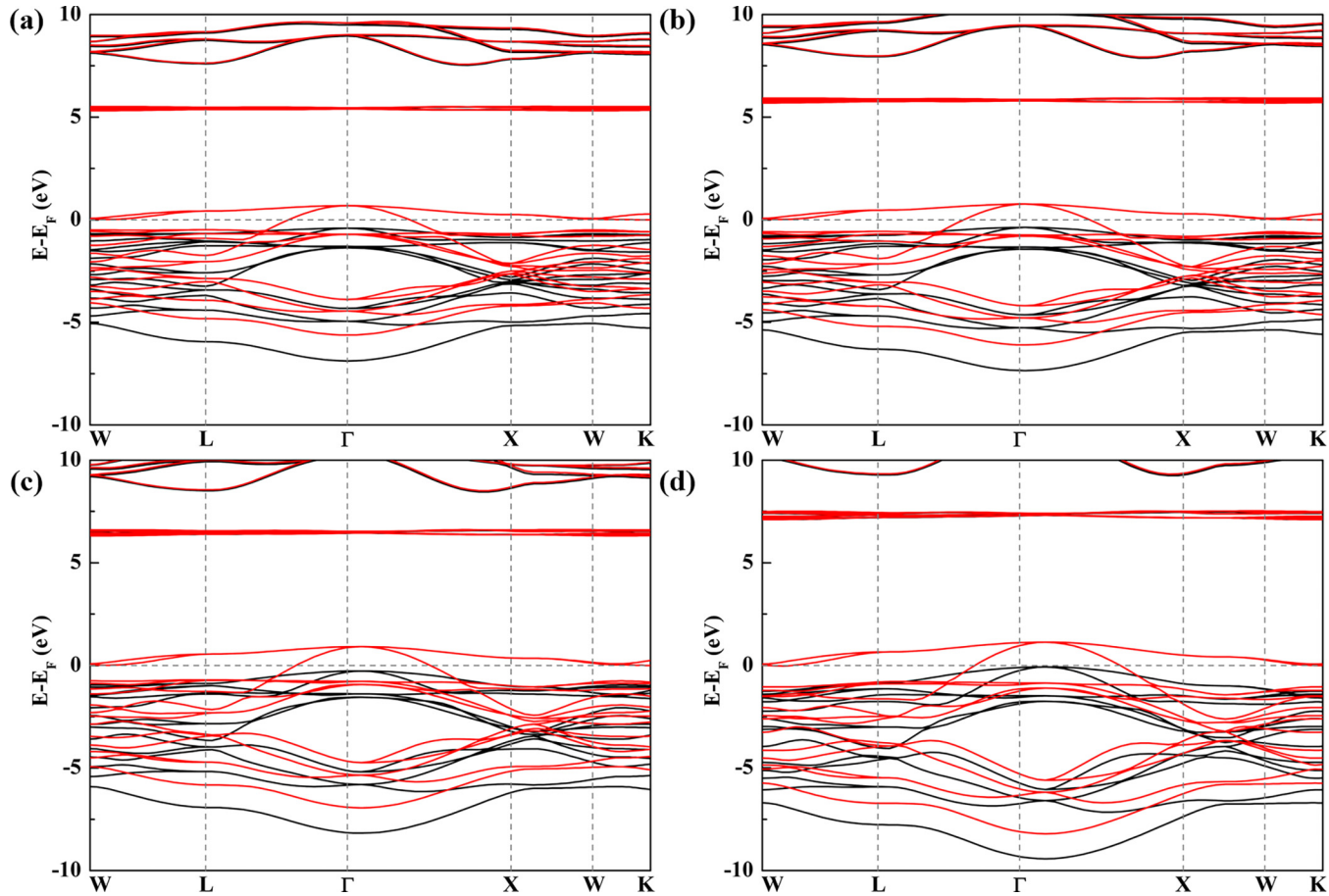

FIG. 5. The electron band structures of F-43m-LaF_5 with spin polarization at (a) 14 GPa, (b) 25 GPa, (c) 50 GPa, and (d) 100 GPa. The spin-up and spin-down channels are black solid lines and red solid lines, respectively.

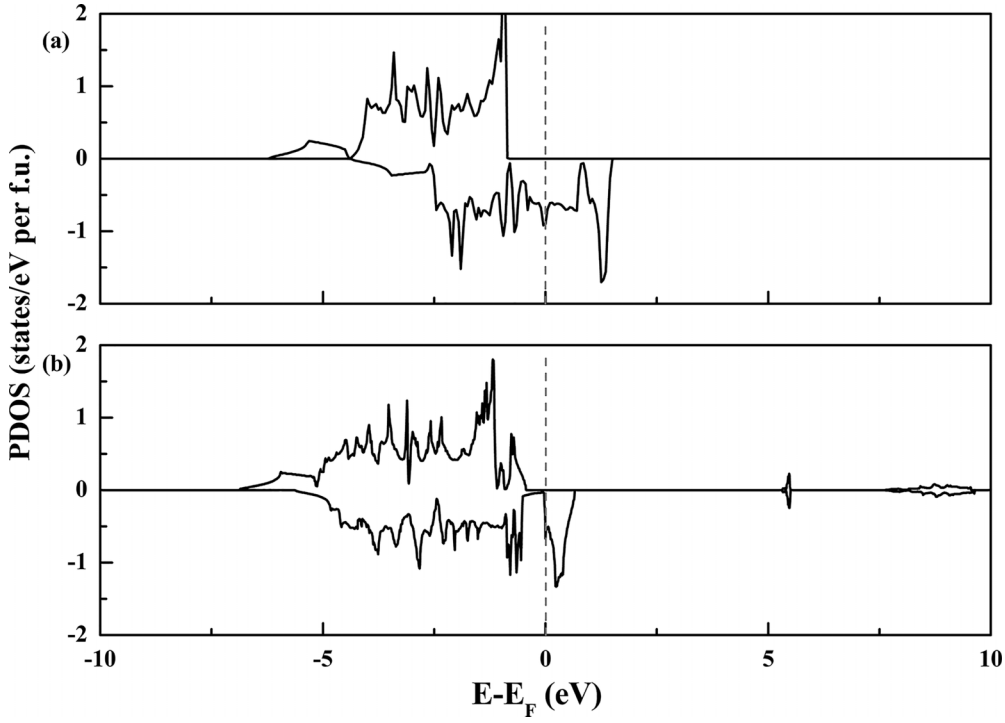

FIG. 6. The partial electron density of states (PDOS) of $2p$ orbitals of $(F_t)_4$ units (a) without and (b) with the interactions between LaF_c framework.

and $1.8e^-$ for the spin-down channel. In $LaF_c(F_t)_4$, all the spin-up channels of $2p$ states still maintain fully occupied ($3e^-$), and the electrons from La transform to the spin-down channel. The IPDOS of the spin-down channel increases to $2.5e^-$, which reduces the total magnetic moment to about $2\mu_B$ and retains the half-metallic character. The large band gap benefits the stability of the pure spin polarization at elevated temperatures. The band gap of predicted $LaF_c(F_t)_4$ is 5.73 eV at 14 GPa, which is comparable to the previously reported 1.60–2.38 eV of ACrZ (A = Li, Na, and K) [55]. As pressure increases, the band gap of the spin-up channel gradually increases to 6.96 eV at 100 GPa. The Curie temperature is also roughly estimated in mean field approximation (MFA) [56]: $T_{curie} = 2\Delta E/3k_B$ where ΔE is the total energy difference between the antiferromagnetic and ferromagnetic states ($\Delta E = E_{AFM} - E_{FM}$) and k_B is the Boltzmann constant. The T_{curie} of $La(F_t)_4F_c$ here is about 674 K at 14 GPa and 505 K at 100 GPa, correspondingly. Until now, more than 1000 Heusler alloys and Heusler derivatives have been discovered with compositions spanning most of the Periodic Table [57]. However, fluorides are rarely included. The pressure-synthesized LaF_5 suggests further efforts are needed for exploring novel fluorine-based binary Heusler derivatives.

D. Superconductivity

LaF_6 is always metallic in the whole investigated pressure range (Fig. S8 [33]). Since the $P6/mcc$-F and La element are both superconductive [47,58], the superconductivity of LaF_6 is expected for further investigation. The phonon band structures, partial phonon density of states (PHDOS), corresponding Eliashberg spectral functions $\alpha^2F(\omega)$, and integral EPC parameters λ as a function of the frequency of LaF_6 are calculated at 50 GPa (Fig. 7). In terms of the PHDOS and $\alpha^2F(\omega)$, the EPC is mainly contributed by the low-frequency range corresponding to the vibration of heavy La atoms. The phonon band structure shows that the phonon softening of the acoustic branch is found at the A, H, and M points. Therefore, the EPC of $R3$-LaF_6 mainly comes from La atoms. At 50 GPa, the EPC parameter λ and logarithmic average phonon frequency ω_{log} are 0.81 and 105.99 K, respectively. According to the McMillan equation, the T_c values of LaF_6 are calculated to be 4.08−5.04 K, which is comparable to 9.3 K of La at the same pressure [58] and 1.3 K of $P6/mcc$-F at 3 TPa [47].

IV. CONCLUSION

To summarize, we performed a systematic investigation on the RE fluorides La-F system by first-principles calculations. The traditional compound LaF_3 is insulating and experiences a phase transition from $Pmmn$ to $Cmmm$ at 141 GPa. The predicted F-$43m$-LaF_5 synthesized above 120 GPa is a binary derivative of the half-Heusler alloys. From 14 to 100 GPa, LaF_5 is half-metallic with a large band gap of the spin-up channel ranging 5.7−6.9 eV from 14 to 100 GPa, which is mainly induced by the F atoms in the tetrahedron units. The Curie temperature is estimated to be 674−505 K at 14 − 100 GPa. The novel $R3$-LaF_6 with layer-stacked structure is superconductive with T_c of about 5 K at 50 GPa. The EPC is mainly provided by the phonon softening of the acoustic branch contributed by La vibrations. Our results reveal various LaF_n compounds with different properties, which indicates the potential for exploring a diversity of novel functional materials in REF_n at high pressures. Further investigations on high-pressure RE-F systems are still needed.

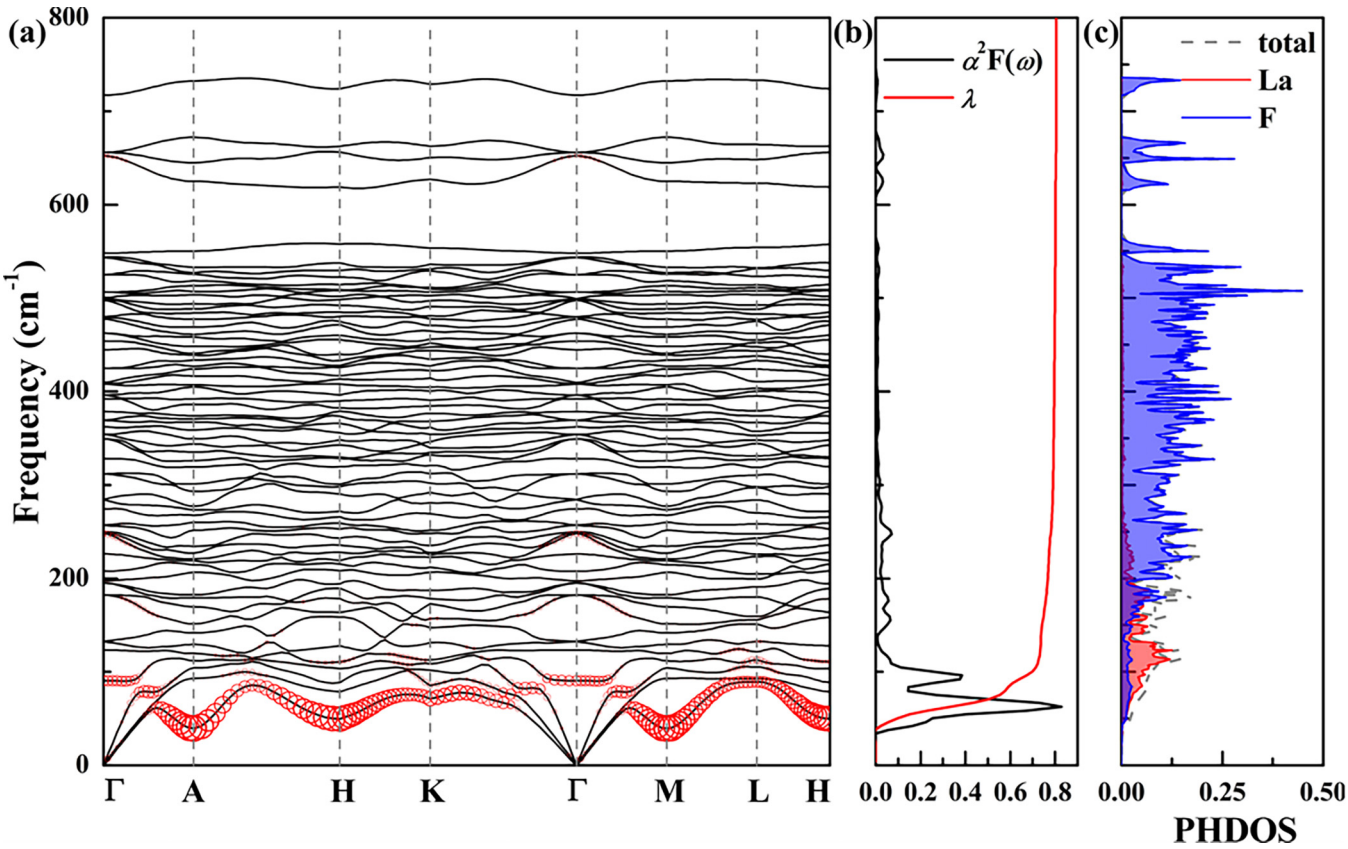

FIG. 7. (a) The phonon band structure, (b) Eliashberg spectral function α^2F(ω), and (c) PHDOS for $R3$-LaF_6 at 50 GPa. Red solid circles represent the electron-phonon parameter $\lambda_{q,j}(\omega)$ of each mode (q, j). The radii of red solid circles are proportional to their respective strength. The integral EPC parameter λ as a function of frequency is calculated and shown in red solid lines.

ACKNOWLEDGMENTS

This work was supported by the "Pioneer" and "Leading Goose" R&D Program of Zhejiang Province under Grant No. 2022C01053, the National Natural Science Foundation of China (Grant No. 12004090), the Zhejiang Provincial Natural Science Foundation of China (Grants No. LQ23A040010 and No. LQ21A050001), and the Fundamental Research Funds for the Provincial Universities of Zhejiang (Grant No. GK219909299001-012).

[1] K. Seppelt, Molecular hexafluorides, Chem. Rev. **115**, 1296 (2015).

[2] M. Rahm, R. Cammi, N. W. Ashcroft, and R. Hoffmann, Squeezing all elements in the periodic table: Electron configuration and electronegativity of the atoms under compression, J. Am. Chem. Soc. **141**, 10253 (2019).

[3] L. Zhang, Y. Wang, J. Lv, and Y. Ma, Materials discovery at high pressures, Nat. Rev. Mater. **2**, 17005 (2017).

[4] J. Lin, S. Zhang, W. Guan, G. Yang, and Y. Ma, Gold with +4 and +6 Oxidation States in AuF_4 and AuF_6, J. Am. Chem. Soc. **140**, 9545 (2018).

[5] J. Lin, X. Du, M. Rahm, H. Yu, H. Xu, and G. Yang, Exploring the limits of transition-metal fluorination at high pressures, Angew. Chem. Int. Ed. **59**, 9155 (2020).

[6] J. Botana, X. Wang, C. Hou, D. Yan, H. Lin, Y. Ma, and M. S. Miao, Mercury under pressure acts as a transition metal: Calculated from first principles, Angew. Chem. Int. Ed. **54**, 9280 (2015).

[7] D. Luo, J. Lv, F. Peng, Y. Wang, G. Yang, M. Rahm, and Y. Ma, A hypervalent and cubically coordinated molecular phase of IF_8 predicted at high pressure, Chem. Sci. **10**, 2543 (2019).

[8] J. Lin, Z. Zhao, C. Liu, J. Zhang, X. Du, G. Yang, and Y. Ma, IrF_8 molecular crystal under high pressure, J. Am. Chem. Soc. **141**, 5409 (2019).

[9] Y. Bai, Z. Liu, L. J. He, F. Ortega, R. Khleif, Y. Chen, Y. Sun, D. D. Yan, and M. Miao, Prediction of core electron reactivity and high oxidation states in radium under high pressure, J. Phys. Chem. C **126**, 12944 (2022).

[10] D. Luo, Y. Wang, G. Yang, and Y. Ma, Barium in high oxidation states in pressure-stabilized barium fluorides, J. Phys. Chem. C **122**, 12448 (2018).

[11] M. S. Miao, Caesium in high oxidation states and as a p-block element, Nat. Chem. **5**, 846 (2013).

[12] D. de Faoite, I. Tobin, A. Ulyanov, O. Roberts, B. Shortt, L. Hanlon, S. McBreen, and K. Stanton, Growth of trigonal

gadolinium fluoride in a glass-ceramic for scintillation and optical applications, J. Eur. Ceram. Soc. **38**, 4739 (2018).
[13] P. S. Campbell, C. Lorbeer, J. Cybinska, and A. V. Mudring, One-pot synthesis of luminescent polymer-nanoparticle composites from task-specific ionic liquids, Adv. Funct. Mater. **23**, 2924 (2013).
[14] Z. Guo, S. Ye, X. Qiao, and D. Wang, Luminescence properties and tunable emission of Ag NCs in oxyfluoride glass through REF_3 (RE = Y, La and Gd) doping, J. Am. Ceram. Soc. **101**, 732 (2018).
[15] J. W. Stouwdam and F. C. van Veggel, Near-infrared emission of redispersible Er^{3+}, Nd^{3+}, and Ho^{3+} doped LaF_3 nanoparticles, Nano Lett. **2**, 733 (2002).
[16] A. Shalav, B. Richards, T. Trupke, K. Krämer, and H. U. Güdel, Application of $NaYF_4$: Er^{3+} up-converting phosphors for enhanced near-infrared silicon solar cell response, Appl. Phys. Lett. **86**, 013505 (2005).
[17] S. V. Eliseeva and J. C. G. Bünzli, Lanthanide luminescence for functional materials and bio-sciences, Chem. Soc. Rev. **39**, 189 (2010).
[18] J. C. G. Bünzli, Lanthanide luminescence for biomedical analyses and imaging, Chem. Rev. **110**, 2729 (2010).
[19] A. Zalkin and D. Templeton, The crystal structures of YF_3 and related compounds, J. Am. Chem. Soc. **75**, 2453 (1953).
[20] W. Xu, W. X. Ji, Y. X. Qiu, W. E. Schwarz, and S. G. Wang, On structure and bonding of lanthanoid trifluorides LnF_3 (Ln = La to Lu), Phys. Chem. Chem. Phys. **15**, 7839 (2013).
[21] A. Cheetham, B. Fender, H. Fuess, and A. Wright, A powder neutron diffraction study of lanthanum and cerium trifluorides, Acta Crystallogr., Sect. B **32**, 94 (1976).
[22] A. Zalkin, D. H. Templeton, and T. E. Hopkins, The atomic parameters in the lanthanum trifluoride structure, Inorg. Chem. **5**, 1466 (1966).
[23] I. Ranieri, S. Baldochi, and D. Klimm, The phase diagram GdF_3–LuF_3, J. Solid State Chem. **181**, 1070 (2008).
[24] W. A. Crichton, P. Bouvier, B. Winkler, and A. Grzechnik, The structural behaviour of LaF_3 at high pressures, Dalton Trans. **39**, 4302 (2010).
[25] T. Dyuzheva, L. Lityagina, G. Demishev, and N. Bendeliani, Phase transition and compressibility of LaF_3 under pressures up to 40 GPa, J. Alloys Compd. **335**, 59 (2002).
[26] T. Dyuzheva, L. Lityagina, G. Demishev, and N. Bendeliani, High-Pressure phase transitions of LaF_3 and CeF_3, Inorg. Mater. **39**, 1198 (2003).
[27] P. Modak, A. Verma, S. Ghosh, and G. Das, Pressure-induced phase transition in tysonite LaF_3, J. Phys. Chem. Solids **70**, 922 (2009).
[28] B. Sahoo, K. Joshi, and S. C. Gupta, Ab initio study on pressure induced structural sequence in LaF_3 up to 2 Mbar, Indian J. Phys. **91**, 535 (2017).
[29] E. Diniz and C. Paschoal, Structural phase transitions under pressure in rare earth triuorides compounds with tysonite structure, Solid State Commun. **136**, 538 (2005).
[30] Z. Sui, J. Wang, D. Huang, X. Wang, R. Dai, Z. Wang, X. Zheng, Z. Zhang, and Q. Wu, Orthorhombic-to-hexagonal phase transition of REF_3 (RE = Sm to Lu and Y) under high pressure, Inorg. Chem. **61**, 15408 (2022).
[31] A. R. Oganov and C. W. Glass, Crystal structure prediction using ab initio evolutionary techniques: Principles and applications, J. Chem. Phys. **124**, 244704 (2006).
[32] A. O. Lyakhov, A. R. Oganov, H. T. Stokes, and Q. Zhu, New developments in evolutionary structure prediction algorithm USPEX, Comput. Phys. Commun. **184**, 1172 (2013).
[33] See Supplemental Material at http://link.aps.org/supplemental/10.1103/PhysRevB.108.064411 for the calculation details of the structure searching by USPEX, the effect of SOC, the equation of states of *Pmmn*-LaF_3 calculated by VASP and Quantum ESPRESSO, the enthalpies of LaF_3, LaF_5, and LaF_6 with respect to other selected related structures under pressure, the ELFs of predicted phases, the phonon band structures of all the predicted structures at corresponding pressures, the oxidation state analysis of La in LaF_5 and LaF_6, the phonon band structures of LaF_5 at different pressures, the band structures of LaF_6 at different pressures, the elastic constants of all the predicted compounds under pressure, and the structure information of all the predicted phases under different pressures. The Supplemental Material also contains Refs. [4,7,8,10,11,14,19–32,34–39,48,59,60].
[34] T. Jarlborg, G. Anderson, B. Sundqvist, and O. Rapp, Resistivity, band structure and superconductivity of DHCP and FCC La under pressure, J. Phys.: Condens. Matter **1**, 8407 (1989).
[35] L. Chen, T. Liang, Z. Zhang, H. Song, Z. Liu, Q. Jiang, Y. Chen, and D. Duan, Phase transitions and properties of lanthanum under high pressures, J. Phys.: Condens. Matter **34**, 204005 (2022).
[36] Q. Lv, X. Jin, T. Cui, Q. Zhuang, Y. Li, Y. Wang, K. Bao, and X. Meng, Crystal structures and electronic properties of solid fluorine under high pressure, Chin. Phys. B **26**, 076103 (2017).
[37] J. P. Perdew, K. Burke, and M. Ernzerhof, Generalized Gradient Approximation Made Simple, Phys. Rev. Lett. **77**, 3865 (1996).
[38] G. Kresse and J. Furthmüller, Efficiency of ab-initio total energy calculations for metals and semiconductors using a plane-wave basis set, Comput. Mater. Sci. **6**, 15 (1996).
[39] G. Kresse and D. Joubert, From ultrasoft pseudopotentials to the projector augmented-wave method, Phys. Rev. B **59**, 1758 (1999).
[40] A. Togo, F. Oba, and I. Tanaka, First-principles calculations of the ferroelastic transition between rutile-type and $CaCl_2$-type SiO_2 at high pressures, Phys. Rev. B **78**, 134106 (2008).
[41] Z. J. Wu, E. J. Zhao, H. P. Xiang, X. F. Hao, X. J. Liu, and J. Meng, Crystal structures and elastic properties of superhard IrN_2 and IrN_3 from first principles, Phys. Rev. B **76**, 054115 (2007).
[42] R. Dronskowski and P. E. Bloechl, Crystal orbital Hamilton populations (COHP): Energy-resolved visualization of chemical bonding in solids based on density-functional calculations, J. Phys. Chem. **97**, 8617 (1993).
[43] R. F. W. Bader, Atoms in molecules, Acc. Chem. Res. **18**, 9 (1985).
[44] P. B. Giannozzi, S. Baroni, N. Bonini, M. Calandra, R. Car, C. Cavazzoni, D. Ceresoli, G. L. Chiarotti, M. Cococcioni, I. Dabo *et al.*, QUANTUM ESPRESSO: A modular and open-source software project for quantum simulations of materials, J. Phys.: Condens. Matter **21**, 395502 (2009).
[45] P. B. Allen and R. C. Dynes, Transition temperature of strong-coupled superconductors reanalyzed, Phys. Rev. B **12**, 905 (1975).
[46] K. Elphick, W. Frost, M. Samiepour, T. Kubota, K. Takanashi, H. Sukegawa, S. Mitani, and A. Hirohata, Heusler alloys for spintronic devices: Review on recent development and future perspectives, Sci. Technol. Adv. Mater. **22**, 235 (2021).

[47] D. Duan, Z. Liu, Z. Lin, H. Song, H. Xie, T. Cui, C. J. Pickard, and M. Miao, Multistep Dissociation of Fluorine Molecules Under Extreme Compression, Phys. Rev. Lett. **126**, 225704 (2021).

[48] F. Mouhat and F. X. Coudert, Necessary and sufficient elastic stability conditions in various crystal systems, Phys. Rev. B **90**, 224104 (2014).

[49] G. A. Landrum and R. Dronskowski, The Orbital Origins of Magnetism: From Atoms to Molecules to Ferromagnetic Alloys, Angew. Chem. Int. Ed. **39**, 1560 (2000).

[50] M. Katsnelson, V. Y. Irkhin, L. Chioncel, A. Lichtenstein, and R. A. de Groot, Half-metallic ferromagnets: From band structure to many-body effects, Rev. Mod. Phys. **80**, 315 (2008).

[51] R. De Groot, F. Mueller, P. v. van Engen, and K. Buschow, New Class of Materials: Half-metallic Ferromagnets, Phys. Rev. Lett. **50**, 2024 (1983).

[52] Y. Lu, X. Li, G. Gong, G. Xiao, A. Gupta, P. Lecoeur, J. Sun, Y. Wang, and V. Dravid, Large magnetotunneling effect at low magnetic fields in micrometer-scale epitaxial $La_{0.67}Sr_{0.33}MnO_3$ tunnel junctions, Phys. Rev. B **54**, R8357 (1996).

[53] E. Y. Tsymbal, O. N. Mryasov, and P. R. LeClair, Spin-dependent tunnelling in magnetic tunnel junctions, J. Phys.: Condens. Matter **15**, R109 (2003).

[54] J. H. Park, E. Vescovo, H. J. Kim, C. Kwon, R. Ramesh, and T. Venkatesan, Direct evidence for a half-metallic ferromagnet, Nature (London) **392**, 794 (1998).

[55] T. T. Hoang, S. Rhim, and S. Hong, Robust half-metallicities of alkali-metal-based half-Heusler compounds, Phys. Rev. Mater. **6**, 055001 (2022).

[56] K. Sato, P. Dederichs, H. Katayama Yoshida, and J. Kudrnovský, Exchange interactions in diluted magnetic semiconductors, J. Phys.: Condens. Matter **16**, S5491 (2004).

[57] J. K. Kawasaki, S. Chatterjee, P. C. Canfield, and G. Editors, Full and half-Heusler compounds, MRS Bull. **47**, 555 (2022).

[58] W. Chen, D. V. Semenok, I. A. Troyan, A. G. Ivanova, X. Huang, A. R. Oganov, and T. Cui, Superconductivity and equation of state of lanthanum at megabar pressures, Phys. Rev. B **102**, 134510 (2020).

[59] K. Rotereau, D. Ph, A. Desert, and J. Y. Gesland, The high-temperature phase transition in samarium fluoride : Structural and vibrational investigation, J. Phys.: Condens. Matter **10**, 1431 (1998).

[60] J. Lin, Q. Yang, X. Li, X. Zhang, F. Li, and G. Yang, Pressure-stabilized hexafluorides of first-row transition metals, Phys. Chem. Chem. Phys. **24**, 1736 (2022).